



Effect of residual surface stress on parametrically excited nonlinear dynamics and instability of double-walled nanobeams: an analytical study

Farzad Ebrahimi¹ · S. Hamed S. Hosseini¹

Received: 20 July 2019 / Accepted: 22 October 2019 / Published online: 29 January 2020
© Springer-Verlag London Ltd., part of Springer Nature 2020

Abstract

A class of nonlinear Mathieu–Hill equation is established to determine the bifurcations and the regions of nonlinear dynamic instability of a short double-walled nanobeam, while the emphasis is placed on investigating the effect of residual surface stress on instability. To achieve this goal, first, a short double-walled nanobeam is modeled and embedded on a viscoelastic foundation and subjected to an axial parametric force. Second, based on the nonlocal elasticity and nonlinear von Karman beam theories, the nonlinear governing equation of motion is derived. Finally, Galerkin technique and multiple time scales method are used to solve the equation. Numerical examples are treated which show various discontinuous bifurcations. Also, infinitely stable and unstable solutions are addressed.

Keywords Parametric excitation · Surface effect · Double-walled nanobeam · Multiple time scales · Nonlinear dynamics

1 Introduction

Knowledge and application of that knowledge are two different sides of the same coin. Recent advances in the application of nanotechnology have resulted in the manufacture of nanoelectromechanical devices. The attractiveness of them is due to their excellent and distinctive mechanical and electrical properties. Among them, carbon nanotubes (CNTs) have been regarded as a class of smart materials and attracted the attention of many researchers for application in optical transparency [1, 2], resonators [3–5], diagnosis of gas atoms [6], memory devices [7] and composite material [8].

In the following, it has been proved that the mechanical characteristics of nanostructures such as nanobeams are size dependent [9]. An investigation presented by Eringen and Edelen [9] revealed that the classical continuum theory is longer eligible for studying nanostructures. Thanks to recent advances in the technology of nanostructures, many

researchers in their investigations [10–16] applied the nonlocal elasticity theory proposed and developed by Eringen and Edelen [9, 17]. The results emphasize that nanostructures are size dependent and the considered interaction between atoms should not be ignored.

Many studies have treated the problem with the effect of surface energy. It is well-known that due to increasing the ratio of surface area to bulk, the effect of surface energy becomes crucial and significant. Therefore, it should be taken into consideration. It is worth mentioning that after proposing a new theory of surface effects on nanoscale structures by Gurtin and Murdoch [18, 19], great attention was given to surface effects including high-order and residual surface stress in nanostructures. A two-dimensional theory of piezoelectric plates and shells by surface effects was established by Zhang et al. [20, 21]. Recently, Shaat et al. [22] realized that the effect of surface energy should be taken into consideration using Gurtin and Murdoch theory. Developing a continuum model, Dingreville et al. [23] took free surface energy into account and studied the effects of surface layers on the elastic behavior of nanowires. In another study, applying nonlocal strain gradient theory, Lu and his co-workers [24] found that the surface effects can influence the critical buckling at a high length-to-thickness ratio. To achieve this goal, they

✉ Farzad Ebrahimi
febrahimi@eng.ikiu.ac.ir

¹ Department of Mechanical Engineering, Faculty of Engineering, Imam Khomeini International University, Qazvin 3414896818, Iran

developed a size-dependent nanoplate. Effects of surface elasticity and residual surface stress on vibration behavior of microbeams were illustrated by Wang and Feng [25]. Karimi and Shahidi [26] demonstrated the effect of surface energy on buckling analysis of skew nanoplates. It was concluded that by increasing the skew angle, the surface layers have less effect on the buckling of nanoplate. Moreover, emphasizing the surface effects on nonlinear vibration characteristics, Ebrahimi and Hosseini [27] developed a double-layered viscoelastic nanoplate. Flexoelectricity and surface effects on vibration and mechanical behavior of nanoplates were studied by Ebrahimi and Barati [28, 29]. They found that considering the surface effect enhances the stiffness of flexoelectric nanoplate as well as natural frequency. Using couple stress and surface elasticity theories, Shaat and Mohamed [30] investigated the size-dependent results of nonlinear electrostatic model of actuated beams. Mechanical properties and buckling of nanowires incorporating surface elasticity and residual surface tension were investigated by Wang and Feng [31]. Chen et al. [32] modeled a Timoshenko beam to study the effects of surface stresses on the natural frequencies of functionally graded (FG) nanobeams (Table 1).

There are literatures devoted to dynamic instability including linear and nonlinear characteristics. She et al. [33, 34] investigated the effect of nonlinearity on the mechanical characteristics and buckling of FG porous nanobeams. Recently, Krylov and his co-workers [35]

concluded that parametric excitation is able to make a stable region larger and instability of the system considerably depends on the damping coefficient. Wang et al. [36] used CNTs to study the effect of parametric excitation on instability. It was found that parametric excitation produces a gap between positive and negative detuning parameters. Other researches [37–39] also demonstrated the influence of parametric excitation on energy harvesting system. According to their results, amplitude in energy harvesting systems is considerably affected by parametric excitation. Wang [40] and Yan et al. [41] also explained the effect of parametric excitation on the characteristics of beams including Timoshenko beam model. The influence of thermo-magneto-mechanical loads in nonlinear instability of a short nanobeam exposed to an external parametric was conducted by Ghadiri and Hosseini [42]. The above literature survey in dynamic instability of micro/nanostructures clarifies that dynamic instability of micro- and nanostructures has been untouched in many aspects [43, 44].

Motivated by the lack of sufficient accuracy in the effect of residual surface stress on nonlinear dynamics and instability of double-walled nanobeams caused by an axial force producing parametric excitation, in the present study, the effect of considering residual surface stress on nonlinear dynamics and instability of double-walled nanobeams subjected to an external parametric excitation is investigated. A short double-walled nanobeam is modeled

Table 1 Parameter definitions

Symbol	Expression	Symbol	Expression
E	Young's modulus	L	Length of the beam
τ_{kl}	The classical stress tensor	b_1, b_2	Inner and outer width of nanobeam
τ_0	Residual surface stress	h_1, h_2	Inner and outer thickness of nanobeam
E^s	Surface elastic modulus	c	van der Waals coefficient
σ_{xx}	The axial normal stress	A_1, A_2	Cross-sectional area of inner and outer layers
ε_{xx}	The axial normal strain	ε_0	Nonlinear strain vector
μ_1, μ_2	Damping coefficient of inner and outer layers	T_0, T_1	Time scales
σ_1	Detuning parameter of inner layer	c_d	Viscous damping coefficient
σ_2	Detuning parameter of outer layer	δ_1	Parametric excitation amplitude of inner layer
$e_0 a$	Nonlocal parameter	δ_2	Parametric excitation amplitude of outer layer
β_1, β_2	Nonlinearity coefficient of inner and outer layers	I_1, I_2	The moment of inertia of outer and inner layers
ε	Strain vector	k_w	Winkler foundation coefficient
κ	Variation of curvature vector	f_1, f_2	Transverse load
F_1, F_2	Force amplitude	Ω	Frequency excitation
t	Time	ϵ	Scaling parameter
ρ	Mass density	u	Displacement of neutral layer
ω_{10}	Natural frequency of inner layer	w	Nanobeam deflection
ω_{20}	Natural frequency of outer layer		

and embedded on a viscoelastic foundation. In the next step, nonlinear governing equation of motion is derived, while the nonlocal elasticity theory and nonlinear von Karman beam theory are applied. To solve the equations, Galerkin technique and multiple time scales method are employed as well. A class of nonlinear Mathieu–Hill equation is established to analyze the nonlinear instability of the system while the emphasis is placed on study of bifurcations.

2 Problem formulation

In Fig. 1, the schematic of double-walled nanobeam embedded on a viscoelastic foundation under an axial force is shown. For each layer of nanobeam, an axial force is employed as a function with a harmonic excitation with frequency (Ω). The thermo-magneto-mechanical loads are applied to expose the outer layer. Besides, the viscoelastic foundation is a combination of viscous damping coefficient (c_d) and Winkler coefficient (k_w). The length of nanobeam taken is L and the inner and outer diameters of nanobeam are d_i and d_o , respectively.

2.1 Constitutive relations

Referring to the nonlocal elasticity theory presented by Eringen [45, 46], the key idea of the Eringen theory is that the nonlocal stress tensor $\sigma_{kl,l}$ at point X can be defined as below:

$$\sigma_{kl,k} - \rho \ddot{u}_l = 0, \tag{1}$$

$$\sigma_{kl}(X) = \int_V K(X, X') \tau_{kl}(X') dV(X'), \tag{2}$$

$$\sigma_{kl} = \frac{1}{2} (u_{k,l} + u_{l,k}), \tag{3}$$

where $K(X, X')$ is the Kernel function and represents the nonlocal modulus. Eringen [46] demonstrated that it is possible to represent the integral constitutive relation in an equivalent differential form as:

$$(1 - (e_0 a)^2 \nabla^2) \sigma = \tau, \tag{4}$$

where $\nabla^2 = \frac{\partial^2}{\partial x^2}$ is the Laplacian operator. In addition, $(e_0 a)$ is the nonlocal parameter in which e_0 is a constant determined by experiments and proportionate to each material and a denotes internal characteristic length. According to nonlocal constitutive relations, it yields for nanobeams as:

$$\sigma_{xx} - (e_0 a)^2 \frac{\partial^2 \sigma_{xx}}{\partial x^2} = E \varepsilon_{xx}. \tag{5}$$

Here we can define new terms as the axial force and the resultant bending moment so that:

$$\{N, M\} = \int_A \sigma_x(1, z) dA, \tag{6}$$

in which z depicts the transverse coordinate in the deflection direction. The displacements can be written as below:

$$u_1(x, z, t) = u(x, t) - z \frac{\partial w}{\partial x}, u_2 = 0, u_3(x, z, t) = w(x, t). \tag{7}$$

Here applying the nonlinear von Karman strain, it yields:

$$\varepsilon = \varepsilon_0 + z\kappa. \tag{8}$$

Using Eqs. (7) and (8), it yields:

$$\varepsilon_0 = \frac{\partial u}{\partial x} + \frac{1}{2} \left(\frac{\partial w}{\partial x} \right)^2, \kappa = - \frac{\partial^2 w}{\partial x^2}. \tag{9}$$

From Eqs. (6)–(9), it can be written as:

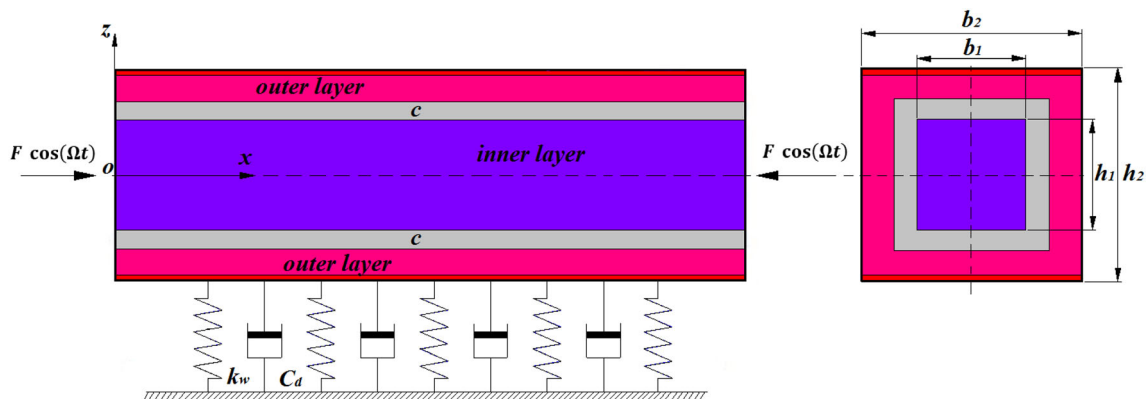


Fig. 1 The double-walled nanobeam embedded in a viscoelastic foundation subjected to parametric excitation

$$\begin{aligned}(1 - (e_0a)^2 \nabla^2)N &= EA\varepsilon_0 \\ (1 - (e_0a)^2 \nabla^2)M &= EI\kappa,\end{aligned}\quad (10)$$

where $I_i = \int z^2 dA_i (i = 1, 2)$. Finally, the equation of motion is derived as follows [47, 48]:

$$\begin{aligned}EI_1 \frac{\partial^4 w_1}{\partial x^4} - \frac{\partial}{\partial x} \left(N_1 \frac{\partial w_1}{\partial x} \right) + (e_0a)^2 \frac{\partial^3}{\partial x^3} \left(N_1 \frac{\partial w_1}{\partial x} \right) \\ + \rho A_1 \frac{\partial^2}{\partial t^2} \left[w_1 - (e_0a)^2 \frac{\partial^2 w_1}{\partial x^2} \right] \\ = f_1 - (e_0a)^2 \frac{\partial^2 f_1}{\partial x^2},\end{aligned}\quad (11a)$$

$$\begin{aligned}EI_2 \frac{\partial^4 w_2}{\partial x^4} - \frac{\partial}{\partial x} \left(N_2 \frac{\partial w_2}{\partial x} \right) + (e_0a)^2 \frac{\partial^3}{\partial x^3} \left(N_2 \frac{\partial w_2}{\partial x} \right) \\ + \rho A_2 \frac{\partial^2}{\partial t^2} \left[w_2 - (e_0a)^2 \frac{\partial^2 w_2}{\partial x^2} \right] \\ = f_2 - (e_0a)^2 \frac{\partial^2 f_2}{\partial x^2},\end{aligned}\quad (11b)$$

in Eqs. (11a) and (11b), $N_i (i = 1, 2)$ are defined as below:

$$N_1 = F_1 \cos \Omega \tilde{t} - \left[\frac{EA_1}{2L} \right] \int_0^L \left(\frac{\partial w_1}{\partial x} \right)^2 dx, \quad (12a)$$

$$N_2 = F_2 \cos \Omega \tilde{t} - \left[\frac{EA_2}{2L} \right] \int_0^L \left(\frac{\partial w_2}{\partial x} \right)^2 dx \quad (12b)$$

in Eqs. (12a), (12b), the term of axial force ($F_i \cos \Omega \tilde{t} (i = 1, 2)$) is the reason of parametric excitation of the nanobeam. In Eqs. (11a) and (11b), $f_i (i = 1, 2)$ is defined as below:

$$f_1 = c(w_1 - w_2), \quad (13a)$$

$$f_2 = k_w w_2 + c_d \frac{\partial w_2}{\partial t} + c(w_2 - w_1). \quad (13b)$$

Compared to bulk atoms in nanostructures, surface atoms have different properties and characteristics so that the surface effects should be considered when there is a high ratio of surface to bulk. It is possible to link surface stress (σ^s) and axial strain (ε_{xx}) by defining the following equation [49]:

$$\sigma^s = \tilde{\tau}_0 + E^s \varepsilon_{xx}. \quad (14)$$

It can be shown that an effective distributed transverse loading along the nanobeam length can be generated by the effects of the residual surface tensions on the surfaces of the Euler–Bernoulli nanobeam [25] so that:

$$q = 2\tilde{\tau}_0 b_i \frac{\partial^2 w_i}{\partial x^2}. \quad (15)$$

Now, for Euler–Bernoulli nanobeam with surface effects, Eq. (10) for the longitudinal force and the nonlocal stress–strain relation can be written as follows [50]:

$$\begin{aligned}N &= (EA_i)^* \left[\int_0^L \left(\frac{\partial w_i}{\partial x} \right)^2 dx \right] + 2\tilde{\tau}_0 b_i \\ M - (e_0a)^2 \frac{\partial^2 M}{\partial x^2} &= (EI_i)^* \frac{\partial^2 w}{\partial x^2}.\end{aligned}\quad (16)$$

Here $(EI_2)^*$ and $(EA_i)^*$ can be expressed as follows [51, 52]:

$$\begin{aligned}(EI_i)^* &= E \left(\frac{b_i h_i^3}{12} \right) + E^s \left[\frac{h_i^3}{6} + \frac{b_i h_i^2}{2} \right], \\ (EA_i)^* &= \frac{EA_i}{2L} + E^s \left[\frac{h_i + b_i}{L} \right], A_i = h_i b_i, i = 1, 2.\end{aligned}\quad (17)$$

According to Eqs. (11a, 11b–17), the governing equation of motion of Euler–Bernoulli nanobeam including surface effects is derived as:

$$\begin{aligned}- (EI_1)^* \frac{\partial^4 w_1}{\partial x^4} - \left\{ F_1 \cos \Omega \tilde{t} - (EA_1)^* \int_0^L \left(\frac{\partial w_1}{\partial x} \right)^2 dx \right\} \frac{\partial^2 w_1}{\partial x^2} \\ + (e_0a)^2 \frac{\partial^4 w_1}{\partial x^4} \left\{ F_1 \cos \Omega \tilde{t} - (EA_1)^* \int_0^L \left(\frac{\partial w_1}{\partial x} \right)^2 dx \right\} \\ + \left(1 - (e_0a)^2 \nabla^2 \right) c(w_1 - w_2) - 2\tilde{\tau}_0 \left[\frac{\partial^2 w_1}{\partial x^2} - (e_0a)^2 \frac{\partial^4 w_1}{\partial x^4} \right] \\ = \rho A_1 \left(\frac{\partial^2 w_1}{\partial t^2} - (e_0a)^2 \frac{\partial^4 w_1}{\partial t^2 \partial x^2} \right),\end{aligned}\quad (18a)$$

$$\begin{aligned}- (EI_2)^* \frac{\partial^4 w_2}{\partial x^4} - \left\{ F_2 \cos \Omega \tilde{t} - (EA_2)^* \int_0^L \left(\frac{\partial w_2}{\partial x} \right)^2 dx \right\} \frac{\partial^2 w_2}{\partial x^2} \\ + c_d \frac{\partial w_2}{\partial t} + k_w w_2 \\ + (e_0a)^2 \frac{\partial^4 w_2}{\partial x^4} \left\{ F_2 \cos \Omega \tilde{t} - (EA_2)^* \int_0^L \left(\frac{\partial w_2}{\partial x} \right)^2 dx \right\} \\ + \left(1 - (e_0a)^2 \nabla^2 \right) c(w_2 - w_1) \\ - 2\tilde{\tau}_0 \left[\frac{\partial^2 w_2}{\partial x^2} - (e_0a)^2 \frac{\partial^4 w_2}{\partial x^4} \right] \\ - (e_0a)^2 k_w \frac{\partial^2 w_2}{\partial x^2} - (e_0a)^2 c_d \frac{\partial^3 w_2}{\partial t \partial x^2} \\ = \rho A_2 \left(\frac{\partial^2 w_2}{\partial t^2} - (e_0a)^2 \frac{\partial^4 w_2}{\partial t^2 \partial x^2} \right).\end{aligned}\quad (18b)$$

Now, nondimensional parameters can be used for better understanding as follows:

$$\begin{aligned}
 X &= \frac{x}{L}, W_i = \frac{w_i}{L}, \gamma = \frac{e_0 a}{L}, K_w = \frac{k_w L^4}{(EI_i)^*}, \\
 C_d &= c_d \sqrt{\frac{L^4}{\rho A_i (EI_i)^*}}, \tau_0 = \frac{\tilde{\tau}_0 b L^2}{(EI_i)^*}, t = \frac{\bar{t}}{L^2} \sqrt{\frac{(EI_i)^*}{\rho A_i}} C = \frac{c L^4}{EI_i} i = 1, 2.
 \end{aligned}
 \tag{19}$$

In Eqs. (18a) and (18b), the Winkler-type foundation is taken from Ref. [53]. Substituting nondimensional parameters into Eqs. (18a) and (18b), it yields:

$$\begin{aligned}
 \frac{\partial^4 W_1}{\partial X^4} &- \left\{ F_1 \cos \Omega t - \int_0^L \left(\frac{\partial W_1}{\partial X} \right)^2 dX \right\} \frac{\partial^2 W_1}{\partial X^2} + \gamma^2 \frac{\partial^4 W_1}{\partial X^4} \\
 &- \left\{ F_1 \cos \Omega t - \int_0^L \left(\frac{\partial W_1}{\partial X} \right)^2 dX \right\} \\
 &- 2\tau_0 \left[\frac{\partial^2 W_1}{\partial X^2} - \gamma^2 \frac{\partial^4 W_1}{\partial X^4} \right] + C(W_1 - W_2) \\
 &- C\gamma^2 \left(\frac{\partial^2 W_1}{\partial X^2} - \frac{\partial^2 W_2}{\partial X^2} \right) \\
 &= \left(\frac{\partial^2 W_1}{\partial t^2} - \gamma^2 \frac{\partial^4 W_1}{\partial t^2 \partial X^2} \right) \\
 \frac{\partial^4 W_2}{\partial X^4} &- \left\{ F_2 \cos \Omega t - \int_0^L \left(\frac{\partial W_2}{\partial X} \right)^2 dX \right\} \frac{\partial^2 W_2}{\partial X^2} \\
 &+ C_d \frac{\partial W_2}{\partial t} + K_w W_2 \\
 &+ \gamma^2 \frac{\partial^4 W_2}{\partial X^4} \left\{ F_2 \cos \Omega t - \int_0^L \left(\frac{\partial W_2}{\partial X} \right)^2 dX \right\} \\
 &- 2\tau_0 \left[\frac{\partial^2 W_2}{\partial X^2} - \gamma^2 \frac{\partial^4 W_2}{\partial X^4} \right] \\
 &- \gamma^2 K_w \frac{\partial^2 W_2}{\partial X^2} - \gamma^2 C_d \frac{\partial^3 W_2}{\partial t \partial X^2} + C(W_2 - W_1) \\
 &- C\gamma^2 \left(\frac{\partial^2 W_2}{\partial X^2} - \frac{\partial^2 W_1}{\partial X^2} \right) \\
 &= \left(\frac{\partial^2 W_2}{\partial t^2} - \gamma^2 \frac{\partial^4 W_2}{\partial t^2 \partial X^2} \right).
 \end{aligned}
 \tag{20a}$$

(20a)

(20b)

For a simply supported double-walled nanobeam, the corresponding boundary conditions would be:

$$W_i = 0, \frac{\partial^2 W_i}{\partial X^2} = 0, \text{ at } X = 0, X = L (i = 1, 2). \tag{21}$$

2.2 Galerkin technique

Now, Galerkin technique is employed to solve the equations so that an approximate solution is substituted into

Eqs. (20a) and (20b). Therefore, the approximate solution is assumed as follows:

$$W_j(x, t) = \sum_{k=1}^{\infty} \psi_{jk}(t) \sin \frac{k\pi x}{L} \tag{22}$$

In Eq. (22), $\psi(t)$ and $\sin \frac{k\pi x}{L}$ are time-dependent function and the spatial basis function, respectively. It is noted that for fundamental frequency, we assume $k = 1$. Now, substituting Eq. (22) into Eqs. (20a) and (20b), it yields:

$$\ddot{\psi}_1 + \omega_{10}^2 \psi_1 + \beta_1 \psi_1^3 - \delta_1 \cos(\Omega t) \psi_1 - \chi_1 \psi_2 = 0 \tag{23a}$$

$$\ddot{\psi}_2 + \omega_{20}^2 \psi_2 + 2\mu_2 \dot{\psi}_2 + \beta_2 \psi_2^3 - \delta_2 \cos(\Omega t) \psi_2 - \chi_2 \psi_1 = 0, \tag{23b}$$

in Eqs. (23a) and (23b), $\epsilon (\epsilon \ll 1)$ is known as scaling parameter. For other parameters, it can be written as:

$$\begin{aligned}
 \omega_{10}^2 &= \left\{ C + \frac{1}{\left(1 + \gamma^2 \left(\frac{\pi}{L} \right)^2 \right)} \left(\frac{\pi}{L} \right)^4 \right\}, \\
 \omega_{20}^2 &= \left\{ [C + k_w + 2\tau_0] \left(\frac{\pi}{L} \right)^2 + \frac{1}{\left(1 + \gamma^2 \left(\frac{\pi}{L} \right)^2 \right)} \left(\frac{\pi}{L} \right)^4 \right\}, \\
 \beta_1 &= \frac{1}{2} \left(\frac{\pi}{L} \right)^4, \beta_2 = \frac{1}{2} \left(\frac{\pi}{L} \right)^4, \mu_2 = \frac{C_d}{2}, \delta_1 = F_1 \left(\frac{\pi}{L} \right)^2, \\
 \delta_2 &= F_2 \left(\frac{\pi}{L} \right)^2, \chi_1 = \chi_2 = C.
 \end{aligned}
 \tag{24}$$

2.3 Multiple scale method

In this section, to solve Eqs. (23a) and (23b), a set of first-order approximations is applied as [54]. This set of first-order approximations is known as multiple time scales approach and proposed by Nayfeh and Mook [54]. Therefore, it yields:

$$\psi_1(t) = \psi_{10}(T_0, T_1) + \psi_{11}(T_0, T_1) \tag{25a}$$

$$\psi_2(t) = \psi_{20}(T_0, T_1) + \psi_{21}(T_0, T_1). \tag{25b}$$

For T_0 and T_1 in Eqs. (25a) and (25b), we have:

$$T_0 = t, T_1 = \epsilon t. \tag{26}$$

And also, we define operators as:

$$\frac{d}{dT} = \frac{d}{dT_0} + \frac{d}{dT_1} + \dots = D_0 + D_1 + \dots, \tag{27a}$$

$$\frac{d^2}{dT^2} = \frac{d^2}{dT_0^2} + 2 \int \frac{d}{dT_0} \frac{d}{dT_1} + \dots = D_0^2 + 2 \int D_0 D_1 + \dots. \tag{27b}$$

At first, substituting Eqs. (25a), (25b) and (27a), (27b) into Eqs. (23a) and (23b) then, for the coefficients of ϵ^0 and ϵ^1 , it can be obtained as:

$$\epsilon^0 : D_0^2 \psi_{10} + \omega_{10}^2 \psi_{10} = 0 \tag{28a}$$

$$D_0^2 \psi_{20} + \omega_{20}^2 \psi_{20} = 0 \tag{28b}$$

$$\begin{aligned} \epsilon^1 : D_0^2 \psi_{11} + \omega_{10}^2 \psi_{11} \\ = -2D_0 D_1 \psi_{10} - \beta_1 \psi_{10}^3 + \chi_1 \psi_{20} + \delta_1 \psi_{10} \cos \Omega T_0 \end{aligned} \tag{29a}$$

$$\begin{aligned} D_0^2 \psi_{21} + \omega_{20}^2 \psi_{21} = -2D_0 D_1 \psi_{20} - 2\mu_2 D_0 \psi_{20} - \beta_2 \psi_{20}^3 \\ + \chi_2 \psi_{10} + \delta_2 \psi_{20} \cos \Omega T_0. \end{aligned} \tag{29b}$$

To solve Eqs. (28a) and (28b), a general solution may be introduced as:

$$\psi_{10} = A(T_1)e^{i\omega_{10}T_0} + \bar{A}(T_1)e^{-i\omega_{10}T_0}, \tag{30a}$$

$$\psi_{20} = B(T_1)e^{i\omega_{20}T_0} + \bar{B}(T_1)e^{-i\omega_{20}T_0}. \tag{30b}$$

Now, A and B are unknown and \bar{A} and \bar{B} are the complex conjugate of A and B . Using Eqs. (30a), (30b) and substituting in Eq. (28a) and (28b), it yields:

$$\begin{aligned} D_0^2 \psi_{11} + \omega_{10}^2 \psi_{11} = -2i\omega_{10}A'e^{i\omega_{10}T_0} - \beta_1 A^3 e^{3i\omega_{10}T_0} \\ - 3\beta_1 A^2 \bar{A} e^{i\omega_{10}T_0} + \chi_1 B e^{i\omega_{20}T_0} \\ + \frac{1}{2} \delta_1 A e^{i(\Omega+1)T_0} + \frac{1}{2} \delta_1 A e^{i(\Omega-1)T_0} + CC, \end{aligned} \tag{31a}$$

$$\begin{aligned} D_0^2 \psi_{21} + \omega_{20}^2 \psi_{21} = -2i\omega_{20}B'e^{i\omega_{20}T_0} - i\mu_2 \omega_{20} B e^{i\omega_{20}T_0} \\ - \beta_2 B^3 e^{3i\omega_{20}T_0} - 3\beta_2 B^2 \bar{B} e^{i\omega_{20}T_0} + \chi_2 A e^{i\omega_{10}T_0} \\ + \frac{1}{2} \delta_2 B e^{i(\Omega+\omega_{20})T_0} + \frac{1}{2} \delta_2 B e^{i(\Omega-\omega_{20})T_0} + CC. \end{aligned} \tag{31b}$$

It is noted that there will be internal resonance when $\omega_{20} \approx 1$. Now, by definition ($\Omega = 2\omega_{20} + \epsilon\sigma_1$, $\omega_{20} = 1 + \epsilon\sigma_2$) that σ_1 and σ_2 are detuning parameters, we eliminate the secular terms in Eqs. (31a) and (31b).

$$2i\omega_{10}A' + 3\beta_1 A^2 \bar{A} - \chi_1 B e^{i\sigma_2 T_1} - \frac{1}{2} \delta_1 A e^{i(\sigma_1+2\sigma_2)T_1} = 0, \tag{32a}$$

$$2i\omega_{20}B' + i\mu_2 \omega_{20} B + 3\beta_2 B^2 \bar{B} - \chi_2 A e^{-i\sigma_2 T_1} - \frac{1}{2} \delta_2 B e^{i\sigma_1 T_1} = 0 \tag{32b}$$

To define a polar form for A and B as below, one can write:

$$A(T_1) = \frac{1}{2} a_1(T_1) e^{i\lambda_1(T_1)} = \frac{1}{2} a_1 (\cos \lambda_1 + i \sin \lambda_1), \tag{33a}$$

$$B(T_1) = \frac{1}{2} a_2(T_1) e^{i\lambda_2(T_1)} = \frac{1}{2} a_2 (\cos \lambda_2 + i \sin \lambda_2). \tag{33b}$$

Substituting Eqs. (33a), (33b) into Eqs. (32a) and (32b), it yields:

$$a_1' = \frac{1}{2} \chi_1 a_1 \sin \gamma + \frac{\delta_1}{4\omega_{10}} a_1 \sin(\sigma T_1) \tag{34a}$$

$$\begin{aligned} a_1 \gamma' = a_1 \lambda_2' + a_1 \sigma_2 - \frac{3}{4\omega_{10}} \beta_1 a_1^3 + \frac{1}{2\omega_{10}} \chi_1 a_2 \cos \gamma \\ - \frac{\delta_1}{4\omega_{10}} a_1 \cos(\sigma T_1) \end{aligned} \tag{34b}$$

$$a_2' = -\frac{1}{2} \mu_2 a_2 + \frac{1}{2\omega_{20}} \chi_2 a_1 \sin \eta + \frac{\delta_2}{4\omega_{20}} a_2 \sin(\sigma_1 T_1) \tag{35a}$$

$$\begin{aligned} a_2 \eta' = a_2 \lambda_1' - a_2 \sigma_2 - \frac{3}{4\omega_{20}} \beta_2 a_2^3 + \frac{1}{2\omega_{20}} \chi_2 a_1 \cos \eta \\ + \frac{\delta_2}{4\omega_{20}} a_2 \cos(\sigma_1 T_1) \end{aligned} \tag{35b}$$

where,

$$\begin{cases} \gamma = (\lambda_2 - \lambda_1) + \sigma_2 T_1 \\ \sigma = \sigma_1 + 2\sigma_2 \\ \eta = (\lambda_1 - \lambda_2) - \sigma_2 T_1 \end{cases}. \tag{36}$$

According to Eqs. (34a, 34b)–(36), three different cases can occur:

Case I: $a_1 = 0, a_2 \neq 0$

$$9\beta_2^2 a_2^4 + 24\omega_{20} \sigma_2 \beta_2 a_2^2 + 4\omega_{20}^2 \mu_2^2 + 16\omega_{20}^2 \sigma_2^2 - \delta_2^2 = 0 \tag{37}$$

Case II: $a_1 \neq 0, a_2 = 0$

$$9\beta_1^2 a_1^4 - 24\beta_1 \sigma_2 a_1^2 + 16\sigma_2^2 - \delta_1^2 = 0 \tag{38}$$

Case III: $a_1 \neq 0, a_2 \neq 0$

$$9\beta_1^2 a_1^6 - 24\beta_1 \sigma_2 a_1^4 + (16\sigma_2^2 - \delta_1^2) a_1^2 - 4\chi_1 \delta_1 a_2 a_1 - 4\chi_1^2 a_2^2 = 0, \tag{39a}$$

$$9\beta_2^2 a_2^6 + 24\omega_{20} \sigma_2 \beta_2 a_2^4 + (4\omega_{20}^2 \mu_2^2 + 16\omega_{20}^2 \sigma_2^2 - \delta_2^2) a_2^2 - 4\chi_2 \delta_2 a_1 a_2 - 4\chi_2^2 a_1^2 = 0. \tag{39b}$$

Finally, assuming ($\mu_2 > 0$), the stability of the system can be evaluated. Therefore, defining Cartesian form of the solution ($A = \frac{1}{2}(p_1 - iq_1)e^{i\sigma_1 T_1}$, $B = \frac{1}{2}(p_2 - iq_2)e^{i\sigma_2 T_1}$) and based on Eqs. (32a) and (32b), it yields:

$$2i\omega_{10}A' - \chi_1 B e^{i\sigma_2 T_1} - \frac{1}{2} \delta_1 A e^{i(\sigma_1+2\sigma_2)T_1} = 0, \tag{40a}$$

$$2i\omega_{20}B' + i\mu_2 \omega_{20} B - \chi_2 A e^{-i\sigma_2 T_1} - \frac{1}{2} \delta_2 B e^{i\sigma_1 T_1} = 0. \tag{40b}$$

Substituting A and B in Eqs. (40a) and (40b), we rewrite the process of the solution as below:

$$p_1' - \left(\sigma_1 + \frac{\delta_1}{4}\right)q_1 - \frac{\chi_1}{2}q_2 = 0 \tag{41a}$$

$$q_1' + \left(\sigma_1 + \frac{\delta_1}{4}\right)p_1 + \frac{\chi_1}{2}p_2 = 0 \tag{41b}$$

$$p_2' + \frac{\mu_2}{2}p_2 - \left(\sigma_2 + \frac{\delta_2}{4\omega_{20}}\right)q_2 - \frac{\chi_2}{2\omega_{20}}q_1 = 0 \tag{42a}$$

$$q_2' + \frac{\mu_2}{2}q_2 + \left(\sigma_2 + \frac{\delta_2}{4\omega_{20}}\right)p_2 - \frac{\chi_2}{2\omega_{20}}p_1 = 0 \tag{42b}$$

Now, it is assumed and substituted ($p_1 = q_1 = p_2 = q_2 = 0$). Thus, Eqs. (41a), (41b) and Eqs. (42a), (42b) are determined as follows:

$$\Delta = \frac{1}{16\omega_{20}^2} \left(2\delta_1\mu_2^2\sigma_1\omega_{20}^2 + \frac{1}{4}\delta_1^2\mu_2^2\omega_{20}^2 + \delta_1^2\sigma_2^2\omega_{20}^2 + \frac{1}{2}\delta_2\delta_1^2\sigma_2\omega_{20} + 8\delta_1\sigma_1\sigma_2^2\omega_{20}^2 \right. \\ \left. \omega_{20}^2 + 4\delta_2\delta_1\sigma_1\sigma_2\omega_{20} + 8\delta_2\sigma_1^2\sigma_2\omega_{20} + \frac{1}{2}\delta_2^2\delta_1\sigma_1 + \delta_2^2\sigma_1^2 + \frac{1}{16}\delta_2^2\delta_1^2 \right. \\ \left. + 4\mu_2^2\sigma_1^2\omega_{20}^2 + 16\sigma_1^2\sigma_2^2\omega_{20}^2 - \chi_1^2\chi_2^2 \right). \tag{43}$$

The amplitude response for different cases can be derived from Eqs. (37)–(39a, 39b). In addition, whenever, $\Delta > 0$ in Eq. (43), the system is stable and $\Delta < 0$ means the system is unstable. Equations (37)–(39a, 39b) and Eq. (43) emphasize that outer layer of nanobeam plays an important role in nonlinear instability of the inner layer in the system.

3 Results and discussion

In this section, numerical results of the present study are presented and discussed in figures. Anterior to the major discussion of this study, the formulation and the numerical should be checked and validated. To achieve this goal, some available literatures are used to have a comparison between results. In the next step, the numerical results for nonlinear dynamics and instability of double-walled nanobeams are presented while it is focused on the effect of residual surface stress on dynamic instability and bifurcations in nonlinear instability of the system. In addition, material properties of the nanobeam is taken as Young’s modulus $E = 1100$ Gpa, the mass density $\rho = 2.3$ g/cm³, the residual surface stress $\tau_0 = 0.89$ N/m and the surface elasticity $E^s = 1.22$ N/m. Also, the inner and outer diameters of the nanobeam are $d_i = 0.7$ nm and $d_o = 1.4$ nm, respectively.

3.1 Validation of the study

From Fig. 2, the relation between the amplitude response ($\tau\tau$) and detuning parameter (σ) in nonlinear instability of a short nanobeam exposed to an external parametric excitation ($\delta = 6$) is observed. It is noted that $\tau\tau$ is the amplitude

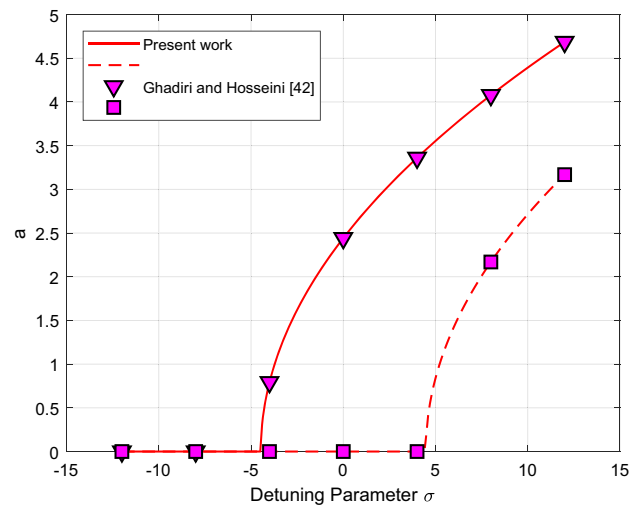


Fig. 2 The relation between amplitude response (a) and detuning parameter (σ) in nonlinear instability of a nanobeam subjected to an external parametric excitation ($\delta = 6$) [42]

response of a single layer nanobeam. In fact, it can be equalized with the amplitude response ($\tau\tau_1$) of the double-layered nanobeam in the present study. The results are also compared with the results presented by Ghadiri and Hosseini [42] is observed. There is a good agreement, as can be observed, between the results. It is found from Fig. 2 that due to parametric excitation, stable (solid line) and unstable (dashed line) curves vary for different values of amplitude response. In Fig. 2, bifurcations happen “out of the clear blue sky” for stable and unstable curves. When the amplitude response is equal to zero, we have two trivial solutions before -5. After that, there is one trivial (unstable) and one non-trivial (stable) solutions until 5. After detuning parameter ($\sigma = 6$), there are two non-trivial stable and unstable solutions. It should be noted that Fig. 2 is achieved when $\delta > 2\mu$ which μ represents the damping coefficient of the system of the single layer nanobeam.

3.2 Numerical results and discussion

As mentioned, in this section, the numerical results of the effect of residual surface stress on nonlinear dynamics and instability of double-walled nanobeam caused by an external axial force is presented while the emphasis is placed on investigating the effect of parametric excitation, residual surface stress effect, viscoelastic foundation coefficients and damping coefficient. To ensure better understanding of nonlinear instability of the system, bifurcations are discussed and identified in plots. Bifurcations can be supercritical pitchfork, subcritical pitchfork and or saddle node. In fact, bifurcations aid in a good view of stable and unstable situations and regions in nonlinear dynamics of the system.

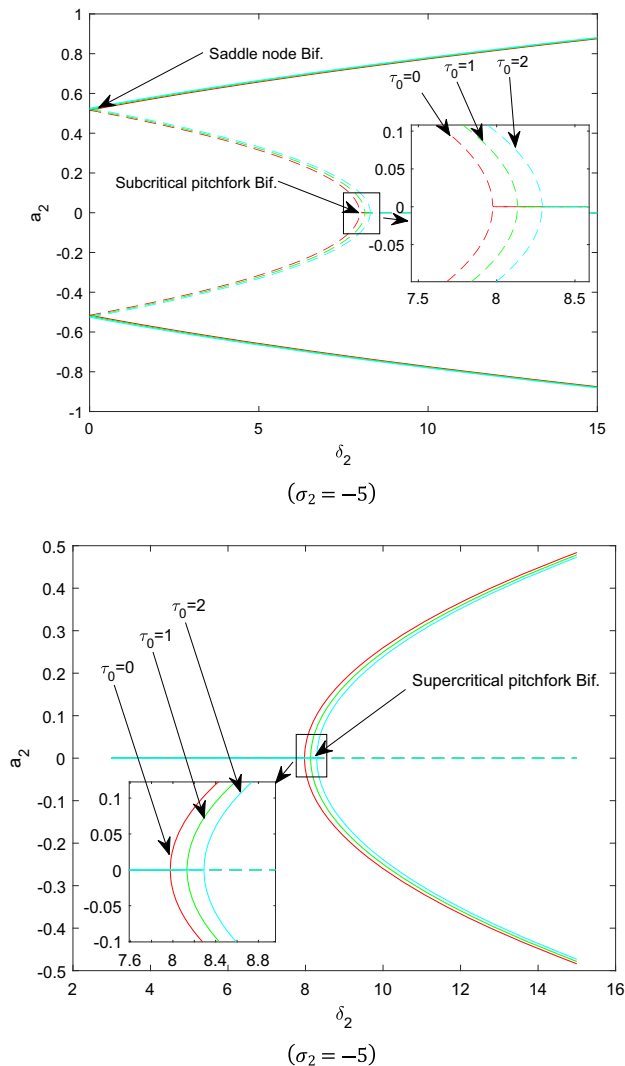


Fig. 3 Effect of residual surface stress on bifurcations in nonlinear instability of the system for various values of force amplitude (δ_2) and amplitude response (a_2)

Figure 3 demonstrates the effect of residual surface stress on bifurcations in nonlinear instability of the system for various values of force amplitude (δ_2) and amplitude response (a_2). As residual surface stress is increased, a shift in bifurcation points is observed so that for negative values of detuning parameter ($\sigma_2 > 0$), it moves to the left side and for positive values of detuning parameter ($\sigma_2 > 0$), it has a tendency to move toward the right side.

The effect of nonlinear coefficient (β_2) on amplitude response (a_2) in nonlinear instability of the system for both with surface stress and without surface stress (τ_0) is displayed in Fig. 4. It would be clear from Fig. 4 that compared to residual surface stress effect, the effect of nonlinear coefficient is completely effective on amplitude response of the system. As a matter of fact, as the nonlinear

coefficient is increased from 1 to 5, the amplitude response considerably grows (Eq. (38)). On the other hand, by considering the surface effect, amplitude response gradually grows. In addition, in both plots, the bifurcations come up with three situations including the saddle node, the supercritical pitchfork and the subcritical pitchfork bifurcations.

From Fig. 5, it is observed that the effect of the foundation coefficients (K_w, C_d) on the amplitude response (a_2) of the system is considerable. It is noted that the residual surface stress is taken $\tau_0 = 1$. In Fig. 5a, it can be seen that as the Winkler coefficient increases from 0 to 100, the subcritical pitchfork bifurcations have a considerable shift along to the left side of the force amplitude (δ_2) axis (Eq. (38)). Therefore, for different values of the Winkler coefficient, different bifurcations include the subcritical pitchfork and the saddle node ones. For Fig. 5b, all explanations of Fig. 5a are valid for Fig. 5b, however, the effects of the viscous damping coefficient are lower than Winkler coefficient on instability of the system. The possible reason of such a behavior is the effect of the foundation coefficients (K_w, C_d) on the natural frequency of the system.

To ensure better understanding of the residual surface stress effect on the nonlinear instability of the system, Fig. 6 presents the emphasis placed on investigating the relation between the amplitude response and the residual surface stress. Figure 6 states the relation between the amplitude response (a_2), the detuning parameter (σ_2) and the force amplitude (δ_2) for different values of the residual surface stress (τ_0) in the nonlinear instability of the system. As the residual surface stress effect is increased, the amplitude response grows. It is worth mentioning that the supercritical pitchfork bifurcation can be seen for various values of the detuning parameter (σ_2). All points on the red line (see, Fig. 6) introduce bifurcation points (the supercritical pitchfork). Figure 6 is derived from Eqs. (39a) and (39b).

In Fig. 7, one of the main results of the present study is observed so that as the force amplitude (δ_1) is increased while other parameters are held constant, stable and unstable curves (dashed lines and solid lines, respectively) move far away and make the gap between them larger. Also, Fig. 7 is obtained from Eq. (37). It means that the stable region (the region between stable and unstable curves) become larger. At the same time, the supercritical and subcritical pitchfork bifurcations would have a shift towards high values of the detuning parameter (σ_2). Moreover, as the force amplitude (δ_1) is increased, the amplitude response slowly decreases.

In contrast to Fig. 7, there is no shift in bifurcations caused by an increase in the nonlinear coefficient (β_1) in Fig. 8 (please see, Eq. (37)). From Fig. 8, it can be revealed that the nonlinear coefficient (β_1) influences the

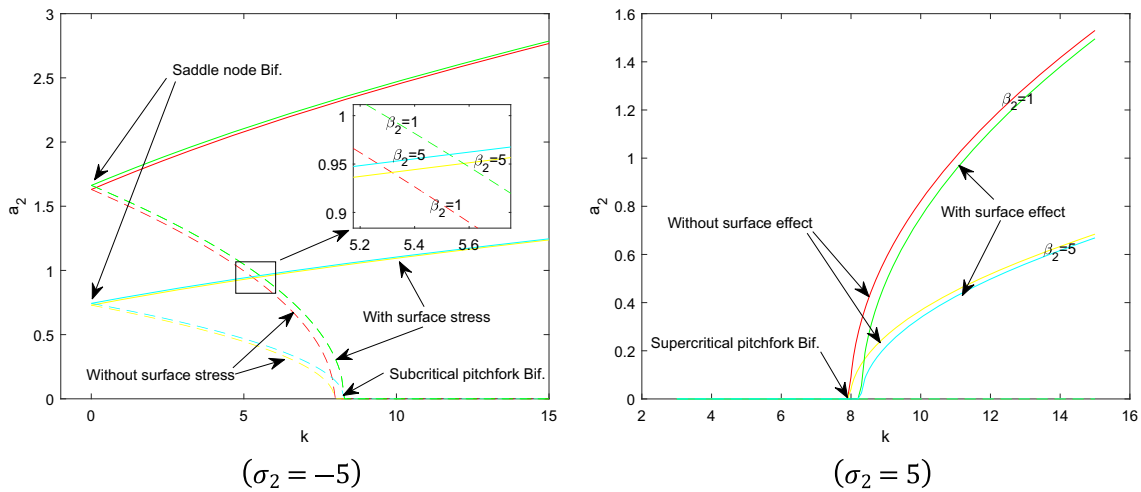


Fig. 4 The effect of the nonlinear coefficient (β_2) on the amplitude response (a_2) in the nonlinear instability of the system for both with the surface stress and without the surface stress (τ_0)

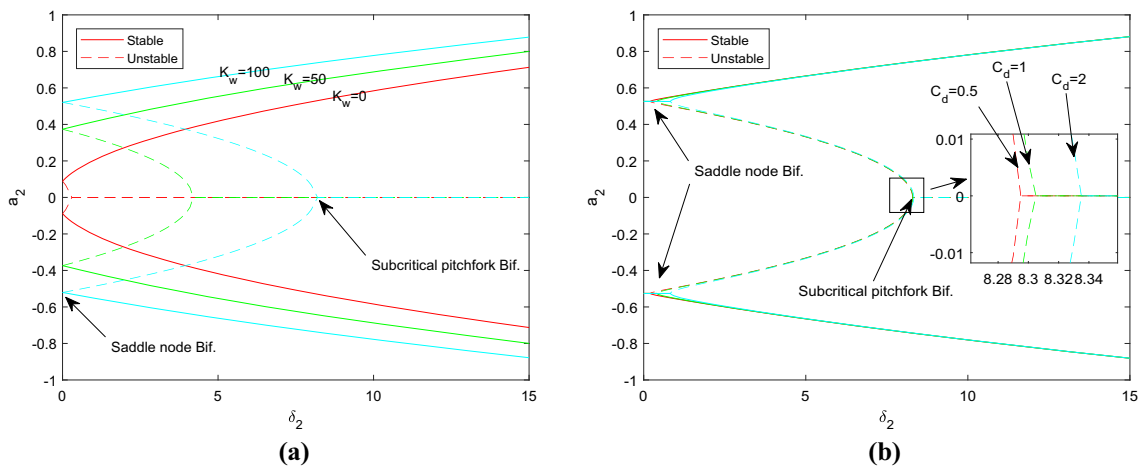


Fig. 5 The effect of foundation coefficients (K_w, C_d) on amplitude response (a_2) in nonlinear instability of the system with residual surface stress ($\tau_0 = 1$)

amplitude response (a_1) in nonlinear instability of the system for different values of detuning parameter (σ_2). As nonlinear coefficient (β_1) is increased, the amplitude response (a_1) considerably decays. It reveals that nonlinearity can have more influence on the mechanical characteristics of double-walled structures than the residual surface stress effect.

The results of the present study in nonlinear dynamics of double-walled nanobeams illustrate this point that compared to single nanobeams [42], double-walled structures such as nanobeams have different nonlinear behavior and bifurcation properties. Furthermore, as can be seen in derived equations and plots, the outer layer has more effect on instability than the inner layer. It seems that the residual surface stress effect on double-walled nanobeams is inevitable in design of nanoelectromechanical devices.

4 Conclusions

As considering all phenomena associated with nanobeams seems to be necessary, the literature is devoted to considering the effect of residual surface stress on nonlinear dynamics and instability of double-walled nanobeams. A class of nonlinear Mathieu–Hill equation is established to determine the bifurcations and the regions of nonlinear dynamic instability of a short double-walled nanobeam while the emphasis is placed on investigating the effect of residual surface stress on instability. In validation of the numerical results, a good agreement between the results of the present study and the results of the available literatures is observed. Numerical examples are treated which show various discontinuous bifurcations. Also, infinitely stable and unstable solutions are addressed. It is noted that

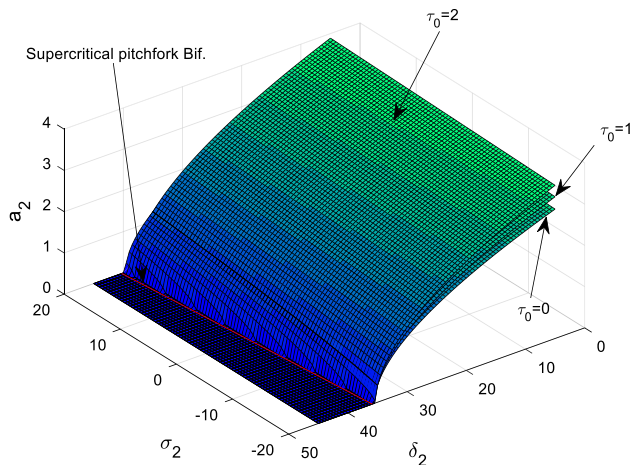


Fig. 6 Relation between amplitude response (a_2), detuning parameter (σ_2) and force amplitude (δ_2) for different values of residual surface stress (τ_0) in nonlinear instability of the system

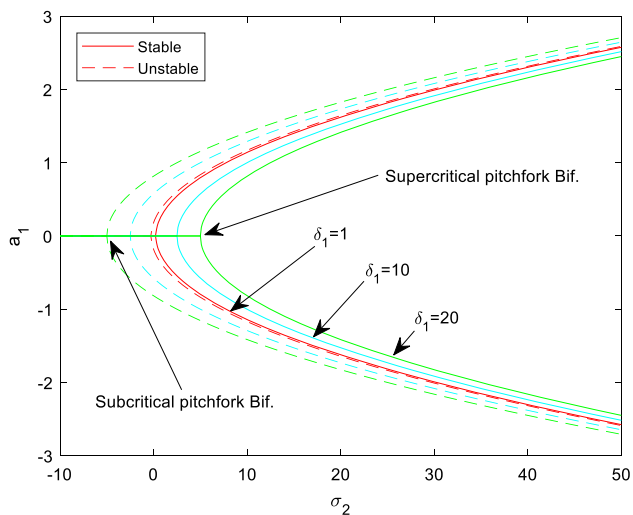


Fig. 7 The effect of force amplitude (δ_1) in nonlinear instability of the system for different values of amplitude response (a_1)

we classify bifurcations as supercritical and subcritical pitchfork and saddle node bifurcations. Some main outcomes of the present study can be enumerated as follows:

- We classify the bifurcations as discontinuous bifurcations.
- All the examples show that a discontinuous bifurcation is always accompanied by a jump.

In addition, the numerical results show that as force amplitude (δ_1) is increased the other parameters are held constant, stable and unstable curves move far away and

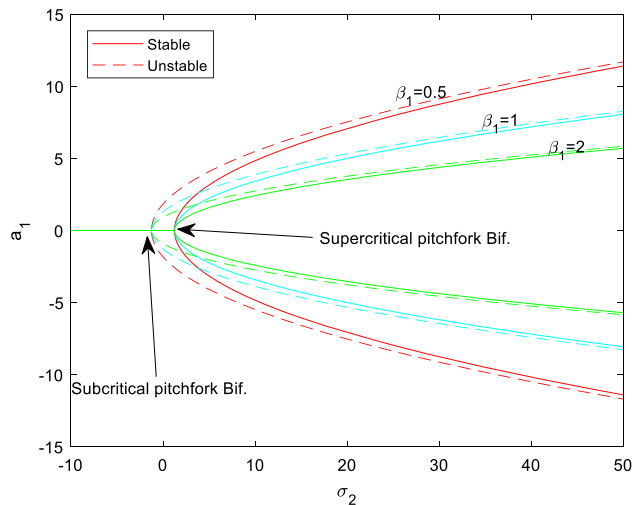


Fig. 8 The effect of nonlinear coefficient (β_1) in nonlinear instability of the system for different values of amplitude response (a_1)

make the gap between them larger. It means that stable region becomes larger.

At the end, we close this paper by stating that considering the residual surface stress effect on nanoscale structures including beams is inevitable in design of the nanoelectromechanical devices.

References

1. Eda G, Fanchini G, Chhowalla M (2008) Large-area ultrathin films of reduced graphene oxide as a transparent and flexible electronic material. *Nat Nanotechnol* 3(5):270
2. Li D, Müller MB, Gilje S, Kaner RB, Wallace GG (2008) Processable aqueous dispersions of graphene nanosheets. *Nat Nanotechnol* 3(2):101
3. Potekin R, Kim S, McFarland DM, Bergman LA, Cho H, Vakakis AF (2018) A micromechanical mass sensing method based on amplitude tracking within an ultra-wide broadband resonance. *Nonlinear Dyn* 92(2):287–304
4. Mahmoud MA (2016) Validity and accuracy of resonance shift prediction formulas for microcantilevers: a review and comparative study. *Crit Rev Solid State Mater Sci* 41(5):386–429
5. Ji Y, Choe M, Cho B, Song S, Yoon J, Ko HC, Lee T (2012) Organic nonvolatile memory devices with charge trapping multilayer graphene film. *Nanotechnology* 23(10):105202
6. Arash B, Wang Q (2013) Detection of gas atoms with carbon nanotubes. *Sci Rep* 3:1782
7. Bunch JS, Van Der Zande AM, Verbridge SS, Frank IW, Tanenbaum DM, Parpia JM, McEuen PL (2007) Electromechanical resonators from graphene sheets. *Science* 315(5811):490–493
8. Kuilla T, Bhadra S, Yao D, Kim NH, Bose S, Lee JH (2010) Recent advances in graphene based polymer composites. *Prog Polym Sci* 35(11):1350–1375
9. Eringen AC, Edelen DGB (1972) On nonlocal elasticity. *Int J Eng Sci* 10(3):233–248

10. Ebrahimi F, Hosseini SHS (2017) Effect of temperature on pull-in voltage and nonlinear vibration behavior of nanoplate-based NEMS under hydrostatic and electrostatic actuations. *Acta Mech Solida Sin* 30(2):174–189
11. Yang Z, Huang Y, Liu A, Fu J, Wu D (2019) Nonlinear in-plane buckling of fixed shallow functionally graded graphene reinforced composite arches subjected to mechanical and thermal loading. *Appl Math Model* 70:315–327
12. Zhang Z, Liu A, Yang J, Huang Y (2019) Nonlinear in-plane elastic buckling of a laminated circular shallow arch subjected to a central concentrated load. *Int J Mech Sci* 161:105023
13. Ebrahimi F, Hosseini SHS, Bayrami SS (2019) Nonlinear forced vibration of pre-stressed graphene sheets subjected to a mechanical shock: an analytical study. *Thin Walled Struct* 141:293–307
14. Ghadiri M, Hosseini SH (2019) Nonlinear forced vibration of graphene/piezoelectric sandwich nanoplates subjected to a mechanical shock. *J Sandw Struct Mater*. <https://doi.org/10.1177/1099636219849647>
15. Shafiei N, She GL (2018) On vibration of functionally graded nano-tubes in the thermal environment. *Int J Eng Sci* 133:84–98
16. Ebrahimi F, Hosseini SHS (2016) Thermal effects on nonlinear vibration behavior of viscoelastic nanosize plates. *J Therm Stresses* 39(5):606–625
17. Eringen AC (1983) Theories of nonlocal plasticity. *Int J Eng Sci* 21(7):741–751
18. Gurtin ME, Murdoch AI (1975) A continuum theory of elastic material surfaces. *Arch Ration Mech Anal* 57(4):291–323
19. Gurtin ME, Murdoch AI (1978) Surface stress in solids. *Int J Solids Struct* 14(6):431–440
20. Zhang C, Chen W, Zhang C (2013) Two-dimensional theory of piezoelectric plates considering surface effect. *Eur J Mech A Solids* 41:50–57
21. Zhang C, Zhu J, Chen W, Zhang C (2014) Two-dimensional theory of piezoelectric shells considering surface effect. *Eur J Mech A Solids* 43:109–117
22. Shaat M, Mahmoud FF, Gao XL, Faheem AF (2014) Size-dependent bending analysis of Kirchhoff nano-plates based on a modified couple-stress theory including surface effects. *Int J Mech Sci* 79:31–37
23. Dingreville R, Qu J, Cherkaoui M (2005) Surface free energy and its effect on the elastic behavior of nano-sized particles, wires and films. *J Mech Phys Solids* 53(8):1827–1854
24. Lu L, Guo X, Zhao J (2019) A unified size-dependent plate model based on nonlocal strain gradient theory including surface effects. *Appl Math Model* 68:583–602
25. Wang GF, Feng XQ (2007) Effects of surface elasticity and residual surface tension on the natural frequency of microbeams. *Appl Phys Lett* 90(23):231904
26. Karimi M, Shahidi AR (2018) Buckling analysis of skew magneto-electro-thermo-elastic nanoplates considering surface energy layers and utilizing the Galerkin method. *Appl Phys A* 124(10):681
27. Ebrahimi F, Hosseini SHS (2017) Surface effects on nonlinear dynamics of NEMS consisting of double-layered viscoelastic nanoplates. *Eur Phys J Plus* 132(4):172
28. Ebrahimi F, Barati MR (2018) Vibration analysis of size-dependent flexoelectric nanoplates incorporating surface and thermal effects. *Mech Adv Mater Struct* 25(7):611–621
29. Ebrahimi F, Barati MR (2019) Dynamic modeling of embedded nanoplate systems incorporating flexoelectricity and surface effects. *Microsyst Technol* 25(1):175–187
30. Shaat M, Mohamed SA (2014) Nonlinear-electrostatic analysis of micro-actuated beams based on couple stress and surface elasticity theories. *Int J Mech Sci* 84:208–217
31. Wang GF, Feng XQ (2009) Surface effects on buckling of nanowires under uniaxial compression. *Appl Phys Lett* 94(14):141913
32. Chen DQ, Sun DL, Li XF (2017) Surface effects on resonance frequencies of axially functionally graded Timoshenko nanocantilevers with attached nanoparticle. *Compos Struct* 173:116–126
33. She GL, Yuan FG, Karami B, Ren YR, Xiao WS (2019) On nonlinear bending behavior of FG porous curved nanotubes. *Int J Eng Sci* 135:58–74
34. She GL, Ren YR, Yan KM (2019) On snap-buckling of porous FG curved nanobeams. *Acta Astronautica* 161:475–484
35. Krylov S, Harari I, Cohen Y (2005) Stabilization of electrostatically actuated microstructures using parametric excitation. *J Micromech Microeng* 15(6):1188
36. Wang YZ, Wang YS, Ke LL (2016) Nonlinear vibration of carbon nanotube embedded in viscous elastic matrix under parametric excitation by nonlocal continuum theory. *Physica E* 83:195–200
37. Alevras P, Theodossiadis S, Rahnejat H (2017) Broadband energy harvesting from parametric vibrations of a class of nonlinear Mathieu systems. *Appl Phys Lett* 110(23):233901
38. Amer YA, El-Sayed AT, Kotb AA (2016) Nonlinear vibration and of the Duffing oscillator to parametric excitation with time delay feedback. *Nonlinear Dyn* 85(4):2497–2505
39. Bobryk RV, Yurchenko D (2016) On enhancement of vibration-based energy harvesting by a random parametric excitation. *J Sound Vib* 366:407–417
40. Wang YZ (2017) Nonlinear internal resonance of double-walled nanobeams under parametric excitation by nonlocal continuum theory. *Appl Math Model* 48:621–634
41. Yan Q, Ding H, Chen L (2015) Nonlinear dynamics of axially moving viscoelastic Timoshenko beam under parametric and external excitations. *Applied Mathematics and Mechanics* 36(8):971–984
42. Ghadiri M, Hosseini SHS (2019) Parametric excitation of Euler–Bernoulli nanobeams under thermo-magneto-mechanical loads: Nonlinear vibration and dynamic instability. *Compos Part B Eng* 173:106928
43. Li C, Lim CW, Yu JL (2010) Dynamics and stability of transverse vibrations of nonlocal nanobeams with a variable axial load. *Smart Mater Struct* 20(1):015023
44. Arani AG, Abdollahian M, Kolahchi R (2015) Nonlinear vibration of a nanobeam elastically bonded with a piezoelectric nanobeam via strain gradient theory. *Int J Mech Sci* 100:32–40
45. Eringen AC (1972) Nonlocal polar elastic continua. *Int J Eng Sci* 10(1):1–16
46. Eringen AC (1983) On differential equations of nonlocal elasticity and solutions of screw dislocation and surface waves. *J Appl Phys* 54(9):4703–4710
47. Emam SA (2009) A static and dynamic analysis of the post-buckling of geometrically imperfect composite beams. *Compos Struct* 90(2):247–253
48. Emam SA, Nayfeh AH (2009) Postbuckling and free vibrations of composite beams. *Compos Struct* 88(4):636–642
49. Gheshlaghi B, Hasheminejad SM (2011) Surface effects on nonlinear free vibration of nanobeams. *Compos B Eng* 42(4):934–937
50. Hosseini-Hashemi S, Nahas I, Fakhher M, Nazemnezhad R (2014) Nonlinear free vibration of piezoelectric nanobeams incorporating surface effects. *Smart Mater Struct* 23(3):035012
51. Ghadiri M, Shafiei N, Akbarshahi A (2016) Influence of thermal and surface effects on vibration behavior of nonlocal rotating Timoshenko nanobeam. *Appl Phys A* 122(7):673

52. Fallah A, Firoozbakhsh K, Kahrobaiyan MH, Pasharavesh A (2011) Nonlinear Free Vibration of Nanobeams With Surface Effects Considerations. In: ASME 2011 International Design Engineering Technical Conferences and Computers and Information in Engineering Conference. American Society of Mechanical Engineers, pp. 191–196
53. Kitipornchai S, He XQ, Liew KM (2005) Continuum model for the vibration of multilayered graphene sheets. *Physical Review B* 72(7):075443
54. Nayfeh AH, Mook DT (2008) *Nonlinear oscillations*. Wiley

Publisher's Note Springer Nature remains neutral with regard to jurisdictional claims in published maps and institutional affiliations.